Heavy ion irradiation damage in $Zr_3(Al_{0.9}Si_{0.1})C_2$ MAX phase

Hassan H. Qarra[1], Kevin M. Knowles[1]*, Mary E. Vickers[1], Eugenio Zapata-Solvas[2], Shavkat Akhmadaliev[3]

[1] Department of Materials Science and Metallurgy, University of Cambridge, 27 Charles Babbage Road, Cambridge, CB3 0FS, UK. *Corresponding author: kmk10@cam.ac.uk .

[2] Department of Materials, Imperial College London, Royal School of Mines, Exhibition Road, London, SW7 2AZ, UK.

[3] Institute of Ion Beam Physics and Materials Research, Helmholtz-Zentrum Dresden-Rossendorf, Bautzner Landstraße 400, Dresden, D-01328, Germany.

Abstract

A $Zr_3(Al_{0.9}Si_{0.1})C_2$ MAX phase-based ceramic with 22% wt. ZrC and 10% wt. Zr_5Si_3 has been irradiated with 52 MeV I^{9+} ions at room temperature, achieving a maximum dose of 8 displacements per atom (dpa). The response of this MAX phase-rich material to irradiation has been studied using scanning electron microscopy, transmission electron microscopy and X-ray diffraction techniques. Post-irradiation examination of the material revealed a number of crystalline changes to the MAX phase. At low doses, $Zr_3(Al_{0.9}Si_{0.1})C_2$ maintained a high degree of crystallinity, while at the highest doses, its degree of crystallinity was reduced significantly. A number of radiation-induced phase transformations were observed, including the decomposition of $Zr_3(Al_{0.9}Si_{0.1})C_2$ into ZrC and other phases, and the formation of β-$Zr_3(Al,Si)C_2$, a MAX phase with a rearranged stacking sequence. Microstructural examination revealed that the majority of the extended defects in $Zr_3(Al_{0.9}Si_{0.1})C_2$ lie in the (0001) basal planes. Analysis of X-ray diffraction profiles after heat treating the 8 dpa-irradiated material for one hour at 300°C and at 600°C showed that there were only subtle changes to the profiles relative to that of the 8 dpa-irradiated material which had not been heat treated. Overall, the experimental results of this study show that the $Zr_3(Al_{0.9}Si_{0.1})C_2$ MAX phase responds less well to irradiation relative to other MAX phases irradiated with high energy heavy ions at room temperature.

1. Introduction

Recent developments in the synthesis of MAX phases have introduced a family that are based on zirconium (Zr) [1–3]. MAX phases are relatively new types of nano-laminated ceramics. Their crystal structure contains strong covalently bonded M-X layers in between weaker M-A metallic bonds. As a consequence, they have properties reflecting aspects of both metals and ceramics [4]. They generally have good electrical and thermal conductivities, good thermal diffusivities, and are oxidation resistant [5]. MAX phases are layered carbides or nitrides with the general formula $M_{n+1}AX_n$, (MAX) where M corresponds to an early transition metal, A to the A-group elements, X is either carbon (C) or nitrogen (N) and n is an integer,

commonly equal to 1, 2 or 3 [6,7]. They have a hexagonal crystal structure belonging to the space group $P6_3/mmc$. One X atom is bonded to 6 M atoms forming an M_6X octahedron. The octahedra alternate with layers of A elements located at the centres of trigonal prisms. The structure of $Zr_3(Al_{0.9}Si_{0.1})C_2$, used in this study, is a $M_3A_1X_2$ (312) type and is illustrated in Fig. 1, where the M, A and X elements are Zr, (Al,Si) and C respectively.

The properties of MAX phases give them the potential to be used as materials in extreme high temperature environments [5,8]. One particular application envisaged is within future nuclear reactors, where they are being considered as candidate materials for cladding components, in both bulk form and as a coating [9]. To date, the majority of MAX phases that have been nominated as materials for nuclear components have been Ti-based, e.g. [10–13], but recent efforts to synthesise MAX phase variations incorporating Zr have been successful, resulting in the synthesis of ceramics containing significant quantities of Zr_2AlC, Zr_3AlC_2 and $Zr_3(Al,Si)C_2$ [1–3]. The significance of Zr in these phases that is of particular relevance for use in nuclear environments is the small thermal neutron absorption cross-section of Zr of 0.185 b, a factor of 33 less than the thermal neutron absorption cross-section of Ti (6.09 b) ([14], Table B.6). Zr alloys are used extensively in current generation nuclear cladding components to maintain a high neutron economy. A high neutron economy enhances the output of the reactor and thus is advantageous economically [15]. Incorporating Zr in MAX phases consequently enhances their potential in to be used as a cladding material. If these phases are to be used in future nuclear environments, it is important that a full understanding of their stability in irradiation intense environments is established.

An efficient way of investigating the possible effects of irradiation of materials in nuclear environments is to use ion accelerators to introduce non-radioactive ions into materials. Because these ions do not activate the atoms in a material, the material does not become radioactive. Therefore, materials can be handled almost immediately after ion irradiation. Although the effects of ions are different from those of neutrons [14,16], the response of a material to ion irradiation can give a good indication of its response to high levels of crystal damage which might arise over years in a nuclear reactor. As Was notes ([16], Ch. 11), radiation damage experiments using ion irradiation allow for easy variation of irradiation parameters to investigate the basic damage processes in materials, and as Linga Murty and Charit observe ([14], p. 267), most radiation effects are universal in nature, regardless of the type of radiation. Consequently, the response to ion irradiation is typically one of the first steps in selecting materials for nuclear applications. Neutron irradiation experiments can then be conducted for further investigation of materials which pass this initial selection process.

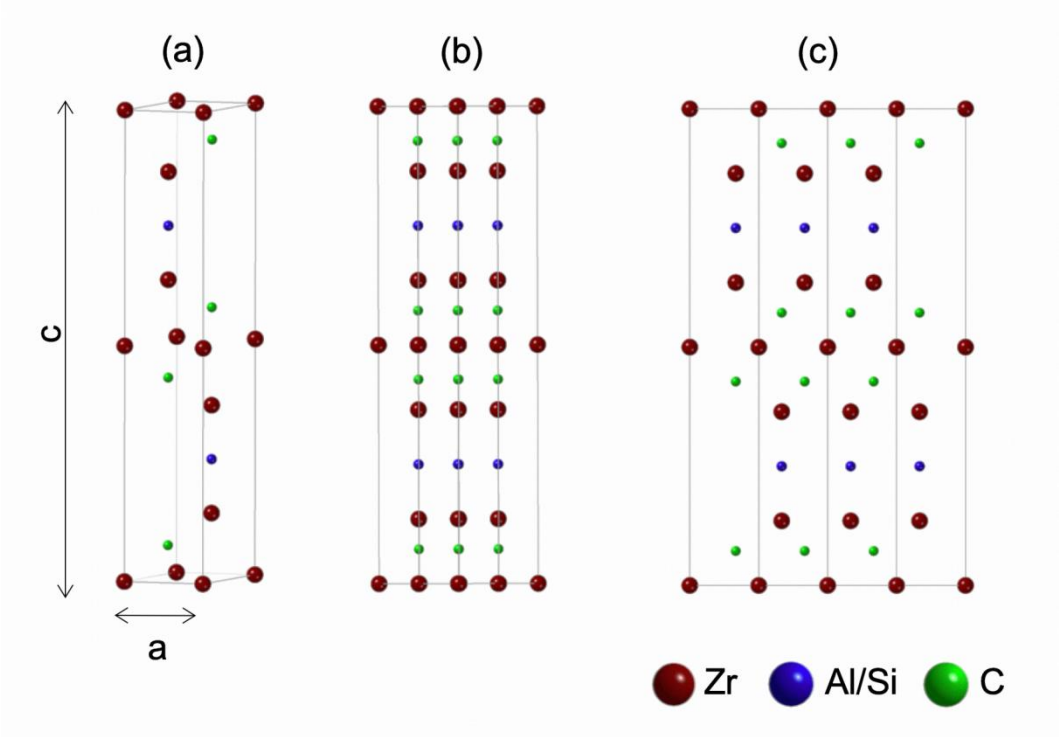

Fig. 1. (a) The unit cell of $Zr_3(Al,Si)C_2$, (b) projection of the layered structure in real space along $[11\bar{2}0]$ and (c) projection of the layered structure in real space along $[1\bar{1}00]$. In each figure the [0001] direction is vertical.

Since the potential of MAX phases for use in irradiation environments was recognised over a decade ago, multiple ion irradiation studies on these materials have been undertaken, almost all of which are on Ti-based MAX phases. From the reported literature on the irradiation of MAX phases, it is apparent that the responses of MAX phases to irradiation generally depend on the exact stoichiometry of the phase, the irradiation temperature, the ion elements and the irradiation energy. Thus, for example, $Ti_3(Si_{0.9}Al_{0.1})C_2$ irradiated with 74 MeV Kr^{20+} and 92 MeV Xe^{23+} ions at room temperature (RT), 300°C and 500°C was shown to develop microstrain and anisotropic changes in lattice parameter, notably expanding preferentially along the *c* axis [17]. This phase was also shown to undergo a partial phase transformation into β-$Ti_3(Si_{0.9}Al_{0.1})C_2$ at high fluences of 1×10^{15} ions/cm^2 for Kr^{20+} irradiation and 5×10^{14} ions/cm^2 for Xe^{23+} irradiation. This transformed phase shares the same space group $P6_3/mmc$, but the *A* element occupies the 2*d* Wyckoff position rather than the 2*b* position [17]. In transmission electron microscopy (TEM) analysis of similar $Ti_3(Si,Al)C_2$ exposed only to room temperature 92 MeV Xe^{23+} ion irradiation at fluence levels up to 2×10^{15} ions cm^{-2}, equating to doses of > 3 dpa in the highest damaged regions, Le Flem et al. found strong evidence of structural disorder within this MAX phase, with an almost complete absence of black dot contrast in bright field TEM images characteristic of dislocation loops of interstitial atoms arising as a direct consequence of radiation damage [18]. By comparison, at lower dpa values of

0.15–0.2 dpa, Le Flem et al. were able to observe black dot contrast readily in bright field TEM images of $Ti_3(Si,Al)C_2$ [18].

In this context, it is relevant to appreciate that radiation damage behaviour in ceramics exposed to a relatively high dpa level can differ significantly from that seen in metallic materials [19]. For low dpa irradiation in ceramics, radiation damage can recover as in metals through Stages I–V described originally by van Bueren from work undertaken on electrical resistivity measurements in plastically deformed metals [20,21]. These five stages involve processes such as self-interstitial cluster formation and migration, vacancy cluster formation, vacancy migration and vacancy annihilation at interstitial loops ([16], Section 5.9). However, for dpa values > 1 dpa, ceramics can respond to irradiation by adopting a more uniformly defective state than occurs in metals [19]. At such values of dpa, phenomena such as swelling and compaction can occur, and also the loss of long-range periodic order, i.e., amorphisation [19]. In a review of the way in which complex non-metallic materials behave in response to radiation damage, Trachenko has suggested that the resistance to amorphisation is defined by the competition between the short-range covalent and long-range ionic forces in these materials [22]. In this respect, covalently bonded ceramics are more prone to amorphisation than ionically bonded ceramics. Thus, for example SiC is readily amorphisable by radiation damage, whereas Si_3N_4 is highly resistant to amorphisation because of the high electronegativity of N in comparison with C [22].

Where it has been possible to undertake neutron irradiation work on Ti-based 312 MAX phases [23–25], macroscopic volumetric swelling is observed as a consequence of a ~ 2 dpa dose of neutrons. The authors explain this in terms of microcracking and kink-band based deformation mechanisms causing an increase in free volume, rather than in terms of defect-based swelling, i.e. as a consequence of swelling of the crystal structure parallel to the *c*-axis and compaction along the *a*-axis, because the volumetric swelling occurred after neutron irradiation at temperatures where lattice parameter dilatation was either absent or significantly reduced relative to lower temperature irradiation [24,25]. In none of these neutron irradiation study was there any report of amorphisation of the Ti-based 312 MAX phases. Interestingly the lower dpa neutron irradiation work of Tallman et al. [23] showed evidence for black spots characteristic of small defect clusters, dislocation loops some 75±25 nm in diameter and triangular defects. A further noteworthy aspect of the Tallman et al. work is the observation of the decomposition of Ti_3AlC_2 and Ti_3SiC_2 into TiC, presumably together with undetected Al- and Si-containing phases.

The relative resistance of Ti-based 312 MAX phases to amorphisation is further confirmed by heavy ion irradiation work reported by Whittle et al. [11], Huang et al. [26] and Clark et al. [27], with Ti_3AlC_2 being observed as being more resistant to

damage than Ti_3SiC_2 by Whittle et al. and Huang et al. for the irradiation procedures that they used. Huang reported $\alpha \rightarrow \beta$ phase transitions in both these 312 phases after 7 MeV Xe^{26+} irradiation to ~ 5–10 dpa levels. The macroscopic swelling manifesting itself as crack formation after room temperature irradiation was interpreted qualitatively by Huang et al. in terms of swelling of the MAX phase crystal structure because such cracks were not visible in material irradiated at 600 °C. The irradiation conditions used by Clark et al. [27] consisted of midrange ion doses of 10–30 dpa achieved using 5.8 MeV Ni^{4+} ions at irradiation temperatures of 400 °C and 700 °C. At these temperatures and doses, the Ti_3SiC_2, Ti_3AlC_2 and Ti_2AlC materials that they examined all remained fully crystalline, albeit with disorder introduced into the *c*-plane stacking sequence of the MAX phases. Here, however, the Ti_3AlC_2 phase exhibited significantly more damage than Ti_3SiC_2, and there was evidence for saturation of radiation damage at levels < 10 dpa as a consequence of migrating interstitials being able to recombine with immobile vacancies under the irradiation conditions that they used. For these elevated temperature irradiation experiments, they were able to demonstrate that the MAX phases behaved in terms of their response like metals between Stage I and Stage III of the van Beuren stage I-V classification as a function of recovery temperature, i.e., between the onset temperature for interstitial motion and the onset temperature for vacancy motion. The cracking that they observed in the samples irradiated at 400 °C was interpreted in terms of stresses being introduced at grain boundaries from of the change in shape of grains as a consequence of *c*-lattice swelling and *a*-lattice contraction of the MAX phases.

Thus, overall, while it is evident that there are differences in the analysis and interpretation of experimental data from one study to the next, in broad terms, a reasonably consistent picture is beginning to emerge of the response to irradiation of the Ti-based MAX phases. By comparison, work on irradiation of Zr-MAX phases is in its very early stages. Prior to the work reported here, there have been two studies, one on Zr_2AlC [28] and one on Zr_3AlC_2 and $(Zr_{0.5}Ti_{0.5})_3AlC_2$ [29]. In the first of these two studies, Zr_2AlC irradiated with Au^{7+} ions was shown to develop significant lattice disorder and partial amorphisation upon irradiation to 3.5 dpa at RT conditions, whereas at 300 °C and 600 °C it exhibited relatively good irradiation resistance [28]. The second study used protons as their source of radiation, with irradiation temperatures of 350 °C and 575 °C [28]. In this second study, *c*-parameter expansion and *a*-parameter contraction were reported in the irradiated samples, reducing as the temperature of irradiation increased, just as in the Ti-MAX phases, with Zr_3AlC_2 shown to be able to exhibit dynamic defect recovery above 400 °C. In addition, they reported is that in the nitrogen-rich atmospheres used for their variable temperature X-ray diffraction work, Zr_3AlC_2 decomposes to ZrC and Zr_3Al_2. A further notable aspect of this work relevant to the study reported here was the relatively low wt% level of the 312 MAX phase in their Zr_3AlC_2 billet [29]: 44 ± 4 wt%, consistent with the work reported by Lapauw et al. in 2016 which reported 61mol% in the

sample that they analysed [1]. Thus, relative to Ti-based 312 MAX phases, phase purity has been an issue for Zr-based 312 material.

The aim of this current study was to investigate the response of $Zr_3(Al,Si)C_2$-based MAX phase ceramics to relatively high levels of ion irradiation damage of the order of a few dpa. This has been achieved by high energy heavy ion irradiation of Zr-MAX phase material at room temperature. Repeated attempts to improve the wt% level of 312 phase in the material used for irradiation studies led to the deliberate incorporation of a small amount of Si into the starting composition because, without the incorporation of Si, wt% levels of 312 phase produced remained stubbornly low [3]. The choice of ion irradiation and irradiation temperature was constrained by beam line availability at the time at the Ion Beam Centre at Helmholtz-Zentrum Dresden-Dusseldorf.

2. Experimental

2.1 Material

The $Zr_3(Al_{0.9}Si_{0.1})C_2$ MAX phase-based material used in this study was synthesised at Imperial College London, UK. Sufficient quantity of this material with a relatively high yield of MAX phase was available for the experiments that are reported in this work. A comprehensive explanation of the synthesis procedure is reported by Zapata-Solvas et al. [3]. In brief, powders of ZrH_2, Al, Si and graphite were mixed and milled by ZrO_2 balls. The mixture was hot pressed at 1500°C for one hour in an inert atmosphere. The bulk material was sectioned into cubes of 5 mm sides and polished on one side to a 0.2 μm finish with an ordinary diamond suspension. The samples were then cleaned using acetone, followed by methanol, in an ultrasonic bath for 10 minutes each. X-ray diffraction (XRD) analysis and Rietveld fitting of powdered material showed that the synthesised material contained 68.2% wt. $Zr_3(Al_{0.9}Si_{0.1})C_2$, 21.6% wt. ZrC, 10.2% wt. Zr_5Si_3 and, potentially, traces of other intermetallic phases, although these could not be detected by XRD. A pseudo-Voigt peak shape model was used for the refinements. Refinements began with the background, scale factors and March–Dollase factor followed by the lattice parameters and peak widths of the MAX phase in the mixture, and then the same for the two other phases. The XRD pattern from the material and the Rietveld fit are both plotted in the graph shown in Fig. 2. The crystal structures of $Zr_3(Al_{0.9}Si_{0.1})C_2$, ZrC and Zr_5Si_3 are each specified by the data shown in Table 1, calibrated using a Si standard. Unfortunately, it was not possible to undertake a detailed Rietveld method analysis on XRD profiles from bulk irradiated material. This is because the analysis of the irradiated XRD profiles was complicated by the presence of high crystal damage, multiple phases and crystal sizes, and the further complication of lattice irradiation-induced strain.

2.2 Irradiation experiments

The ion irradiation experiments were performed on the polished surfaces of the 5 mm cubes at the Ion Beam Centre (IBC) at Helmholtz-Zentrum Dresden-Rossendorf (HZDR), Germany. The irradiation was performed using a 6 MV Tandetron accelerator under high vacuum (3×10^{-6} mbar) [30]. The accelerator supplied a scanning beam of I^{9+} ions at 52 MeV. Irradiation experiments were performed at room temperature (RT) (±20 °C). The sample holder was fixed with thermocouples to allow for the temperature to be monitored during the experiments. There was no cooling during the RT experiments, but, due to the low ion flux, temperatures did not exceed 40 °C. High temperature irradiation was not possible on this particular beam line as it was not fitted with an in-situ heater. Once the irradiation was completed, the chamber was allowed to cool to RT and was vented with nitrogen gas. A full list of the irradiation experiments is shown in Table 2.

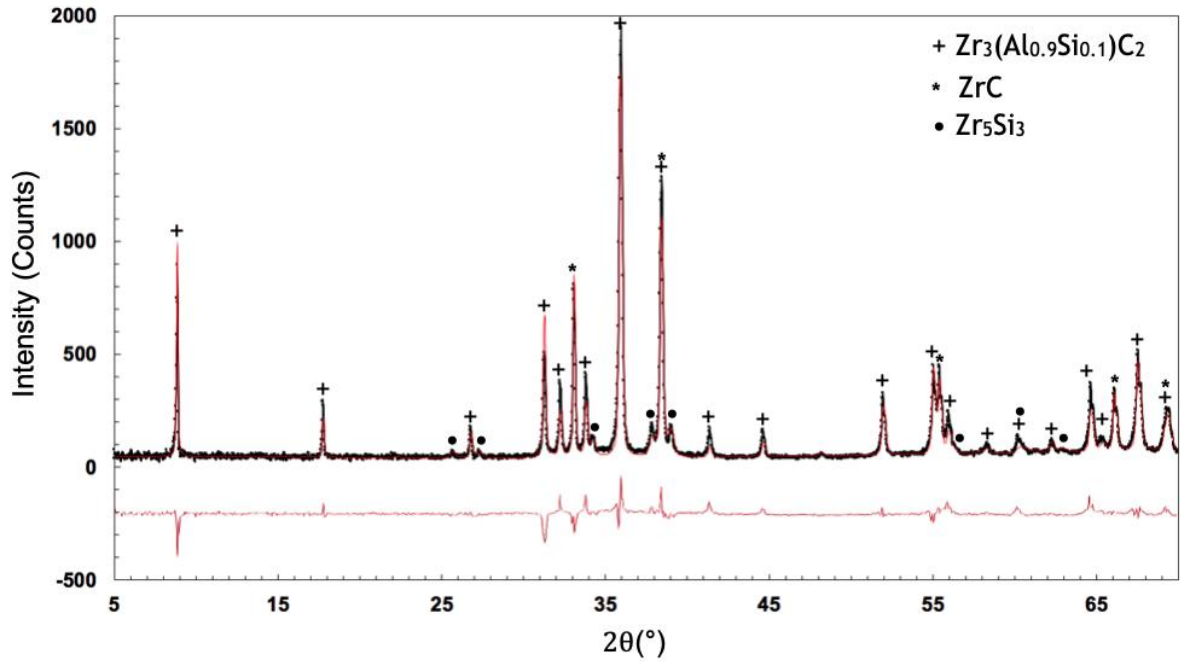

Fig. 2 XRD pattern and Rietveld fit showing the three main phases of the material prior to the irradiation experiments: $Zr_3(Al_{0.9}Si_{0.1})C_2$, ZrC and Zr_5Si_3.

Table 1 Structural Parameters of $Zr_3(Al_{0.9}Si_{0.1})C_2$, ZrC and Zr_5Si_3.

Formula	$Zr_3(Al_{0.9}Si_{0.1})C_2$	ZrC	Zr_5Si_3
Lattice parameters (Å)	*a:* 3.3335(7) Å *c*: 19.943(5) Å	*a:* 4.6848(3) Å	*a:* 7.958(1) Å *c:* 5.563(2) Å
Space group	$P6_3/mmc$ (194)	$Fm\bar{3}m$ (225)	$P6_3/mcm$ (193)
Atomic positions			
Zr	2*a*, 4*f;* $z_{zr} = 0.1355$	4*a*	4*d, 6g;* $x_{Zr} = 0.25$
C	4*f;* $z_C = 0.5722$	4*b*	
Al	2*b*		
Si	2*b*		6*g,* $x_{Si} = 0.61$

Table 2 Irradiation experiment fluences along with corresponding dpa values.

Maximum damage (dpa)	Fluence ($\times 10^{14}$ ions cm^{-2})
1.5	5.7
3.5	13.1
5.0	19.5
8.0	30.6

The ion damage levels in $Zr_3(Al_{0.9}Si_{0.1})C_2$ were estimated by the Monte Carlo simulation programme SRIM 2008. The simulation estimated the dpa values per unit length and the ion implantation depth below the surface. The Kinchin–Pease quick calculation method was used with threshold displacement energies of 40, 25, 20 and 28 keV for Zr, Al, Si and C respectively. The dpa profile for 52 MeV I^{9+} ions against the penetration depth is shown in Fig. 3. It should be noted that the reported damage is the maximum damage in the analysed region, and that it is not uniform throughout the sample.

2.3 Post-irradiation heat treatment

In order to investigate the potential for irradiation damage recovery of $Zr_3(Al_{0.9}Si_{0.1})C_2$, the material irradiated to 8.0 dpa, i.e. the sample irradiated with the most fluence, was cut into two parts. One part was heat treated at 300°C for a dwell time of one hour while the other was heat treated at 600°C, also under vacuum for a dwell time of one hour. The samples were inside the furnace during the heating cycle, which was set to a ramp rate of 20°C min^{-1}. After the heat treatment was complete, the samples were removed from the furnace and allowed to cool from the peak temperature to RT in air.

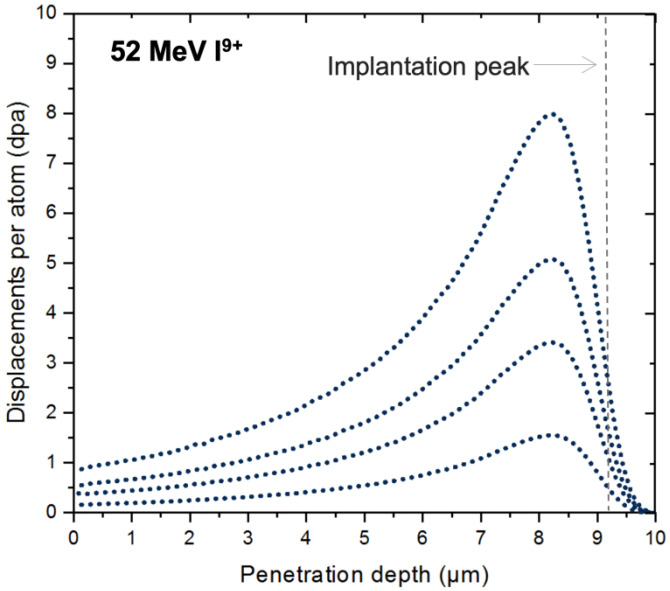

Fig. 3. Estimated damage level profiles (dpa) of $Zr_3(Al_{0.9}Si_{0.1})C_2$ induced by 52 MeV I^{9+} ion irradiation, at various fluences, as a function of ion penetration depth.

2.4 Analytical procedures

A FEI Nova NanoSEM FEG fitted with an Energy Dispersive X-ray (EDX) spectroscope was used to collect backscattered electron and secondary electron images. Thin film lamellae were extracted using a focused ion beam (FIB) instrument (FEI Helios Nanolab Dual Beam FIB SEM). Samples were milled and transferred to copper grids, following the standard lift-out procedure [31]. The films were then milled to a thickness of 100 nm using a 2 kV, 8 pA probe. The very low currents used in the final cleaning step ensured that ion beam artefacts were minimised and did not overshadow effects caused by the irradiation experiments. A JEOL 200CX (Japan) transmission electron microscope was used to obtain bright and dark field images, and selected area diffraction (SAD) patterns. This instrument is fitted with a tungsten electron source and has a maximum operating voltage of 200 kV. The smallest area of analysis was equivalent to that of a circle with a diameter of 500 nm. The camera length was monitored using an Al thin film, which was supplied by Agar Scientific, UK.

A Bruker D8 X-ray diffractometer was used in Bragg–Brentano configuration, which operated in reflection mode at 40 kV and 40 mA with both $CuK_{\alpha1}$ and $CuK_{\alpha2}$ radiation of wavelength 1.5406 Å and 1.5433 Å respectively. A fixed-illuminated length slit was chosen, and the patterns were back-corrected. 8200 steps at three seconds per step were recorded at room temperature from 5^o to 120^o 2θ. This diffractometer is well aligned, so that any zero error should be negligible. However, there could be a small error relating to sample displacement, and this was refined. It is not possible to separate the zero error and sample displacement error unless they are very large

and the data cover a large range in 2θ. For small errors the result in cell parameters is the same whether zero error or sample displacement error is refined. The PANalytical HighScore Plus Version 4.8 software package was used to analyse the diffractometer patterns.

Miller indices have been used to index the X-ray diffraction patterns, in contrast to the transmission electron microscope work reported here, where it is more convenient to use the four-index Miller–Bravais notation for planes and directions. Although the penetration of the X-rays is deeper than the stopping range of I^{9+} ions in $Zr_3(Al_{0.9}Si_{0.1})C_2$, the contribution from the non-irradiated bulk should not affect the comparison between the different irradiated materials.

3. Results

3.1 Microstructure

The topography of the pristine material prior to irradiation experiments is shown in the SEM image in Fig. 4. The material consists mainly of large $Zr_3(Al_{0.9}Si_{0.1})C_2$ grains (approx. 10 × 20 μm) and the two secondary phases: ZrC and Zr_5Si_3. Grains from the two secondary phases decorate the microstructure but are mainly present in small clusters in between larger MAX phase grains. Cracks parallel to the (0001) basal planes of the MAX phase appear on some grains in Fig. 4; these are characteristic of MAX phase materials; they are also observed in pristine Zr_2AlC MAX phase [28] and the pristine Zr_3AlC_2 MAX phase produced by Bowden et al. for their irradiation work [29] . Post-irradiation examination of all the irradiated materials revealed no topographical discrepancies relative to the pristine sample, indicating that the ion irradiation did not alter the topography of the phases noticeably at a micrometre level.

3.2 XRD analysis

XRD patterns collected from the material containing $Zr_3(Al_{0.9}Si_{0.1})C_2$ before and after irradiation to 1.5, 3.5, 5.0, and 8.0 dpa are presented in Fig. 5. The patterns are displayed between 30 and 70^o 2θ: this range covers the majority of the intense diffraction reflections in $Zr_3(Al_{0.9}Si_{0.1})C_2$. Reflections from the secondary and ternary phases, ZrC and Zr_5Si_3 are also marked, as well as a relatively strong peak corresponding to $ZrAl_2$. $ZrAl_2$ is only detectable on patterns obtained from the material irradiated at and above 3.5 dpa. It should be noted that there were no obvious Bragg reflections relating to other phases, although other intermetallic phases may be present, particularly those with similar Bragg reflections to the four phases identified.

From these XRD patterns, it is evident that the heavy ion irradiation has caused a significant modification to the material as a whole, but mostly to the $Zr_3(Al_{0.9}Si_{0.1})C_2$ phase. After irradiation to 1.5 dpa the MAX phase retained a high level of crystallinity, indicated by the sharp diffraction peaks corresponding to the MAX phase. However, the majority of the peaks broaden, most noticeably the 103 reflection. The intensities of reflections along the 00*l* planes also weaken as the irradiation dose increases. Peak broadening suggests the build-up of microstrain along [001]; this is consistent with an accumulation of interstitial point defects introduced into the material as a consequence of the irradiation.

After irradiation to 3.5 dpa, it is clear that the intensities of many of the MAX phase reflections have been reduced, indicating the loss of crystalline long-range order. The appearance of the broad contribution to intensity between 31 and 40° 2θ, typical of amorphous scatter and centred around the most intense 103 peak, is indicative of the loss of crystalline long-range order and corresponds to a large fraction of disordered material. The broad hump is even more prominent at 5.0 dpa, and most noticeable at 8.0 dpa. This trend is consistent with amorphisation behaviour in ceramic materials, with higher irradiation doses resulting in greater loss of crystallinity under the room temperature irradiation conditions used here [19], rather than with the damage saturation behaviour seen after heavy high temperature ion irradiation of irradiated Ti_3AlC_2 and Ti_3SiC_2, where these MAX phases both retain their crystallinity, and where at these elevated temperatures migrating interstitials are able to recombine with immobile vacancies [27]. At both 5.0 and 8.0 dpa, the reflections corresponding to $Zr_3(Al_{0.9}Si_{0.1})C_2$ are increasingly weaker, implying that its layered structure becomes progressively more disordered.

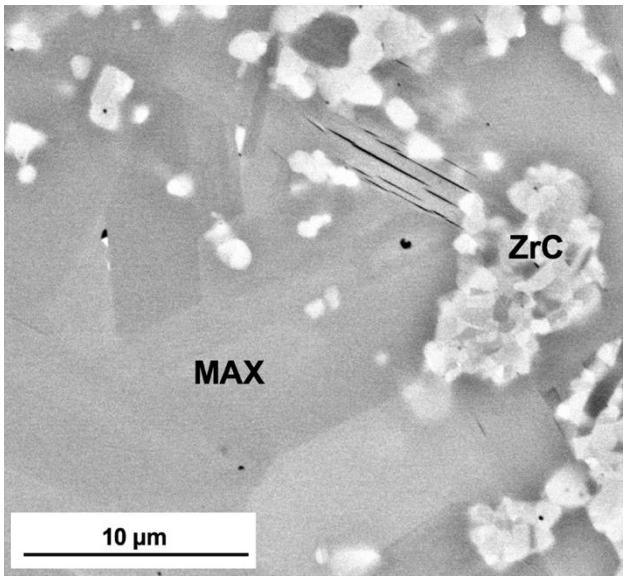

Fig. 4. Backscattered electron (BSE) image of the microstructure of pristine $Zr_3(Al_{0.9}Si_{0.1})C_2$ and ZrC grains. Cracks characteristic of MAX phases can also be seen in some grains, along (0001) planes.

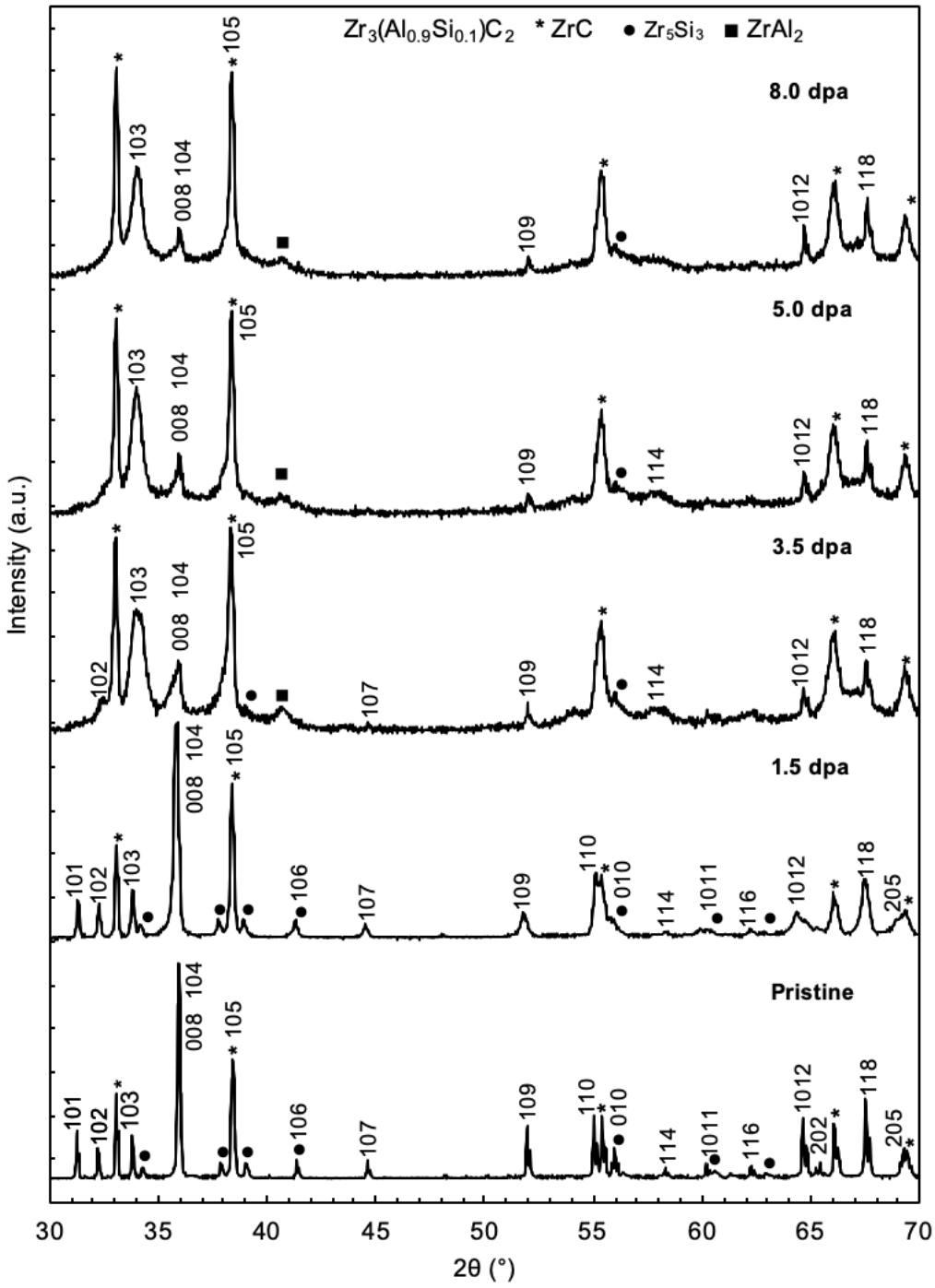

Fig. 5. XRD patterns collected from the material before and after irradiation to 1.5, 3.5, 5.0 and 8.0 dpa at RT.

Alongside the development of disordered material, there is also an increase in the intensity of reflections corresponding to the secondary phase ZrC. This is attributed to the decomposition of $Zr_3(Al_{0.9}Si_{0.1})C_2$. The intensity of ZrC is maintained and increased after irradiation at all doses, suggesting that the MAX phase decomposition is enhanced at progressively higher doses. The extent of damage

between pristine ZrC and the material irradiated to 8.0 dpa is seen in Fig. 5. The broadening of the ZrC peaks at 30.1 and 38.5 ^{o} 2θ suggests that the structure of ZrC is significantly damaged, possibly forming with many structural defects. A new peak appears at 40.7^{o} 2θ upon irradiation to 3.5, 5.0 and 8.0 dpa. This reflection corresponds to a newly developed phase in this material: $ZrAl_2$ or $ZrSi_2$; both of these phases have very subtle differences in relative reflection intensities and peak positions. $Zr(Al/Si)_2$ was not detected in the pristine material and is therefore presumed to develop as a result of the irradiation-induced decomposition of $Zr_3(Al_{0.9}Si_{0.1})C_2$.

Other strong reflections from $Zr(Al/Si)_2$ are also present in the diffraction patterns, but are overshadowed by the MAX phase and the high background of intensity between 30 and 40^{o} 2θ. The reflections from this phase are identified in Fig. 5. It is suggested that this new phase develops from the irradiation of the $Zr_3(Al_{0.9}Si_{0.1})C_2$ and that it is only present in the irradiated material. To maintain overall stoichiometry within the sample, the MAX phase may have also decomposed into other intermetallic phases. However, if such phases were present, they were not detectable by XRD either because they had reflections too close to those of the MAX phase or they had low reflection intensities below the high background present at these high doses. Lattice parameters of the irradiated material were measured at the 1.5 dpa level of irradiation and are shown in Table 3. Unfortunately, XRD profiles from higher doses were judged to have insufficient peaks for accurate measurements. At this 1.5 dpa level of irradiation, the lattice parameters of the MAX phase contract slightly in the *a* parameter but expand notably in the *c* parameter. This trend is consistent with most MAX phases after irradiation and is further discussed in Section 4.

Table 3 Lattice parameter measurements of $Zr_3(Al_{0.9}Si_{0.1})C_2$ before and after 1.5 dpa RT irradiation.

dpa	*a* (Å)	*c* (Å)	% change *a*	% change *c*
0.0	3.332(8)	19.944(3)	-	-
1.5	3.330(3)	20.069(3)	-0.075	+0.631

At progressively higher irradiation doses there is an increase of relative intensity observed in the 102, 103, 105, 106 and 110 reflections while the 101, 104, 107 and 109 reflections reduce in intensity. These intensity changes are consistent with changes observed by Farber et al. in a similar phase, Ti_3SiC_2 [32]. They observed a polymorph of the Ti_3SiC_2 MAX phase identifiable as β-Ti_3SiC_2. This phase belongs to the same space group as the α-Ti_3SiC_2 polymorph, $P6_3/mmc$ (194), where the atom arrangement is the same except that the Si atoms occupy the 2*d* Wyckoff position (2/3,1/3,1/4) rather than the 2*b* position (0,0,1/4). The unit cells of both types in $Zr_3(Al,Si)C_2$ are shown in Fig. 6. Observations from the XRD patterns of irradiated

$Zr_3(Al_{0.9}Si_{0.1})C_2$ compared with simulated XRD patterns using the (Al,Si) component in both the 2*b* and 2*d* Wyckoff positions, shown in Fig. 7, suggests the development and existence of this polymorph in the irradiated material with increasing irradiation dose. The trend in changes of intensity suggests that the irradiation of $Zr_3(Al_{0.9}Si_{0.1})C_2$ leads to the development of β-$Zr_3(Al_{0.9}Si_{0.1})C_2$, a phase which belongs to the space group $P6_3/mmc$ (194), where (Al,Si) atoms occupy the 2d Wyckoff position (2/3,1/3,1/4).

The XRD profiles from the material irradiated to 8.0 dpa heat treated at both 300°C and 600°C respectively along with the non-annealed material irradiated to 8.0 dpa, are shown in Fig. 8. In principle, suitable post-irradiation heat treatment is able to allow irradiation-induced vacancies and interstitials in materials to diffuse and to enable the material to recover its pristine state. However, heat treatment of the sample irradiated to 8.0 dpa for one hour at 300°C only results in minor changes in the XRD reflections from $Zr_3(Al_{0.9}Si_{0.1})C_2$: the (104) peak becomes slightly sharper, and the intensity of the (105), (1,0,12) and (118) peaks are reduced. In addition, no other peaks corresponding to the MAX phase reappear. The relative intensity of the ZrC peaks is also little changed after this heat treatment. XRD reflections from the material heat treated at 600°C for one hour also reveal very little change relative to the XRD pattern from the 8.0 dpa irradiated material. Here, most of the peaks corresponding to $Zr_3(Al_{0.9}Si_{0.1})C_2$ are not changed, except for subtle broadening of the (103) peak. However, $Zr_3(Al_{0.9}Si_{0.1})C_2$ peaks do become sharper.

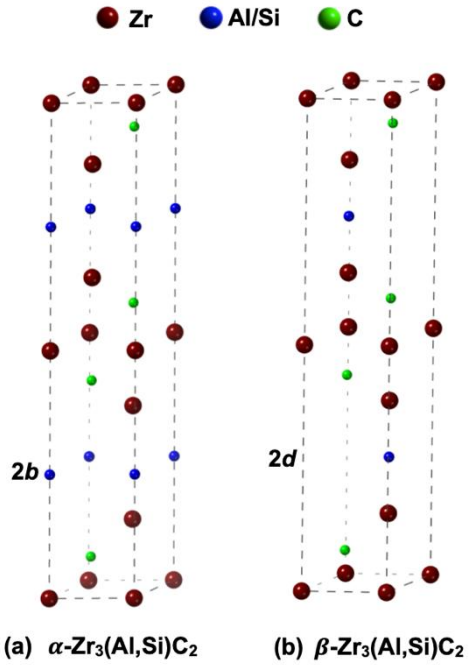

Fig. 6. Unit cells of (a) α-$Zr_3(Al,Si)C_2$ with (Al,Si) atoms in the 2*b* position and (b) β-$Zr_3(Al,Si)C_2$ with (Al,Si) atoms in the 2*d* position.

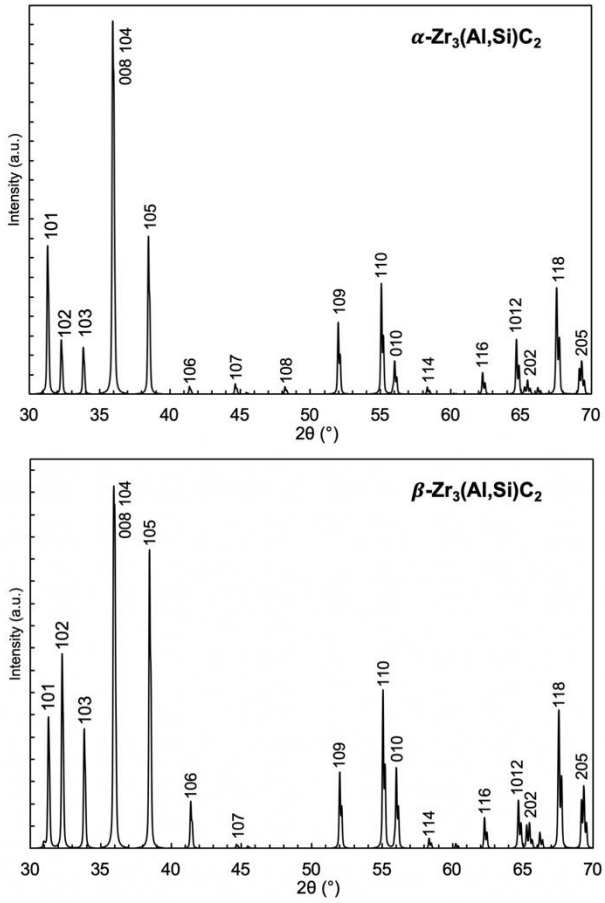

Fig. 7. Simulated XRD patterns from α-$Zr_3(Al,Si)C_2$ with (Al,Si) atoms in the 2*b* position and β-$Zr_3(Al,Si)C_2$ with (Al,Si) atoms in the 2*d* position.

3.3 Transmission electron microscopy (TEM) analysis

3.3.1. MAX phase samples before irradiation

The majority of $Zr_3(Al_{0.9}Si_{0.1})C_2$ grains in material that had not been irradiated were free from defects. However, it was evident that some MAX phase grains had stacking faults (SFs) on the (0001) basal planes, as shown in the TEM micrographs in Fig. 9. The presence of such stacking faults is a characteristic feature of faulted layer carbides – for example, β-silicon carbide whiskers show similar faulting in real space on (111) planes, but on a much more extensive scale, together with very strong streaking in reciprocal space [33]. In those grains where it was evident that there was faulting, some $Zr_3(Al_{0.9}Si_{0.1})C_2$ grains had relatively few SFs, such as the grain in Fig. 9(e), while in other grains such as Fig. 9(a) and Fig. 9(c) a relatively high number of SFs could be seen. These basal plane faults will have been produced during the synthesis process and can be attributed to mistakes in the Zr-Al,Si-C layered structure.

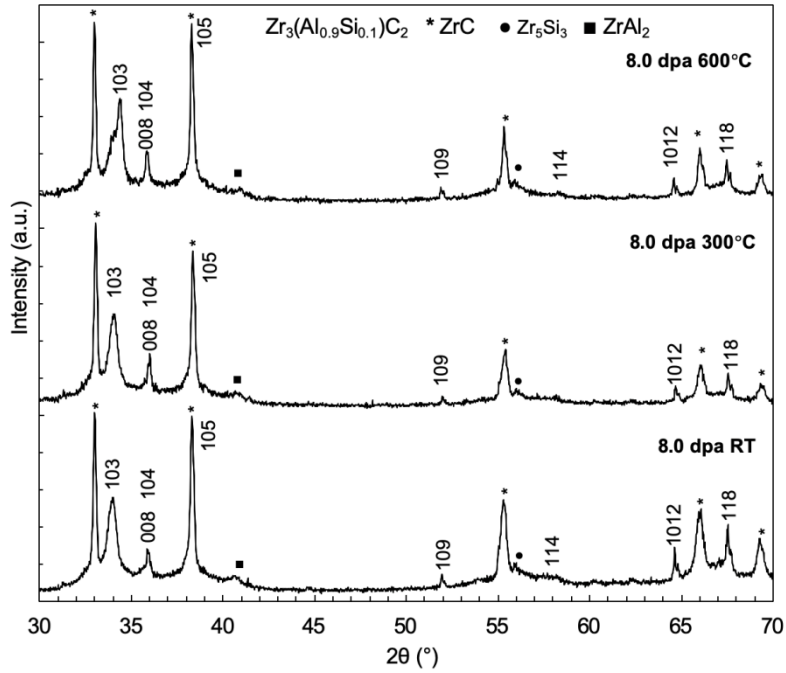

Fig. 8. XRD patterns collected from (i) the material irradiated at RT to 8.0 dpa, (ii) material irradiated at RT and then heat treated at 300 °C for 1 h, and (iii) material irradiated at RT to 8 dpa and then heat treated at 600 °C for 1 h.

3.3.2. MAX phase samples after ion beam irradiation

In this work, attention was focussed on the microstructural changes of MAX phases at a sub-micrometre level present in the thin film lamellae extracted using the FIB – the limited area able to be analysed in such samples and the limitations imposed by the electron microscope used together precluded a more complete study of the irradiated material. As a consequence, it would not have been appropriate to have attempted a detailed analysis of the electron diffraction patterns from the MAX phase for the phase transformation of α-$Zr_3(Al_{0.9}Si_{0.1})C_2$ to β-$Zr_3(Al_{0.9}Si_{0.1})C_2$ predicted by the X-ray work. Furthermore, evidence for the expected amount in the amount of ZrC in the irradiated material could only have been at best qualitative because of the small areas studied – these could well not be characteristic of large areas of irradiated material. Other interesting scientific questions following from the XRD work such as whether the ZrC produced as a consequence of irradiation is different physically and chemically from that in the samples before irradiation, and how Zr_5Si_3 and $ZrAl_2$ form during irradiation will also require further, in-depth studies.

Selected area electron diffraction (SAED) patterns obtained from lamellae extracted from $Zr_3(Al_{0.9}Si_{0.1})C_2$ irradiated at different conditions are shown in Fig. 10. The lamellae were extracted from a depth of 7–8 μm below the surface, which

corresponds to the region of maximum dose (Fig. 3). The selected zone axes were taken to show the diffraction spots along the (000*l*) set of reflections. At increasing irradiation doses, there is a reduction in the intensity of the spots, together with the clear formation of a halo ring. Such halo rings are characteristic of scatter from amorphous or disordered material and are indicative of the loss of long-range atomic order. These observations from SAED patterns of $Zr_3(Al_{0.9}Si_{0.1})C_2$ are therefore consistent with the XRD results at these irradiation doses.

In contrast to irradiated $Zr_3(Al_{0.9}Si_{0.1})C_2$ grains, which as we have noted were almost featureless and without defects, irradiated $Zr_3(Al_{0.9}Si_{0.1})C_2$ grains contained a high number of one- and two-dimensional defects. These defects were mainly stacking faults and dislocation lines. No dislocation loops characteristic of interstitial point defect clusters were observed. Most dislocation lines appeared in arrays and were approx. 500 nm in length in projection seen in these TEM thin sections. Stacking faults along the 000*l* planes propagated across the entire grain length of the MAX phase, shown in Fig. 11a. In Fig. 11b, mid-grain dislocations labelled D1 and D2 pin a stacking fault labelled SF. Other similar dislocations and stacking faults can also be seen along the basal planes.

A high number of defects were observed in $Zr_3(Al_{0.9}Si_{0.1})C_2$ irradiated to 5.0 dpa and 8.0 dpa. Some grains developed a high density of dislocations, while the grains maintained crystallinity. These dislocations formed in parallel arrays, shown in Fig. 12a, while some grains developed stacking faults along the basal planes as well as dislocations, shown in Fig. 12b.

Trace analysis showed that the dislocations lie on the basal planes. Two beam conditions were used to determine the Burgers vector **b** of the dislocations through the invisibility condition **g** • **b** = 0 for suitable diffracting reciprocal lattice vectors **g.** The analysis shown in Fig. 13 suggested that **b** was parallel to $[2\bar{1}\bar{1}0]$, consistent with **b** = $\frac{1}{3}[2\bar{1}\bar{1}0]$.

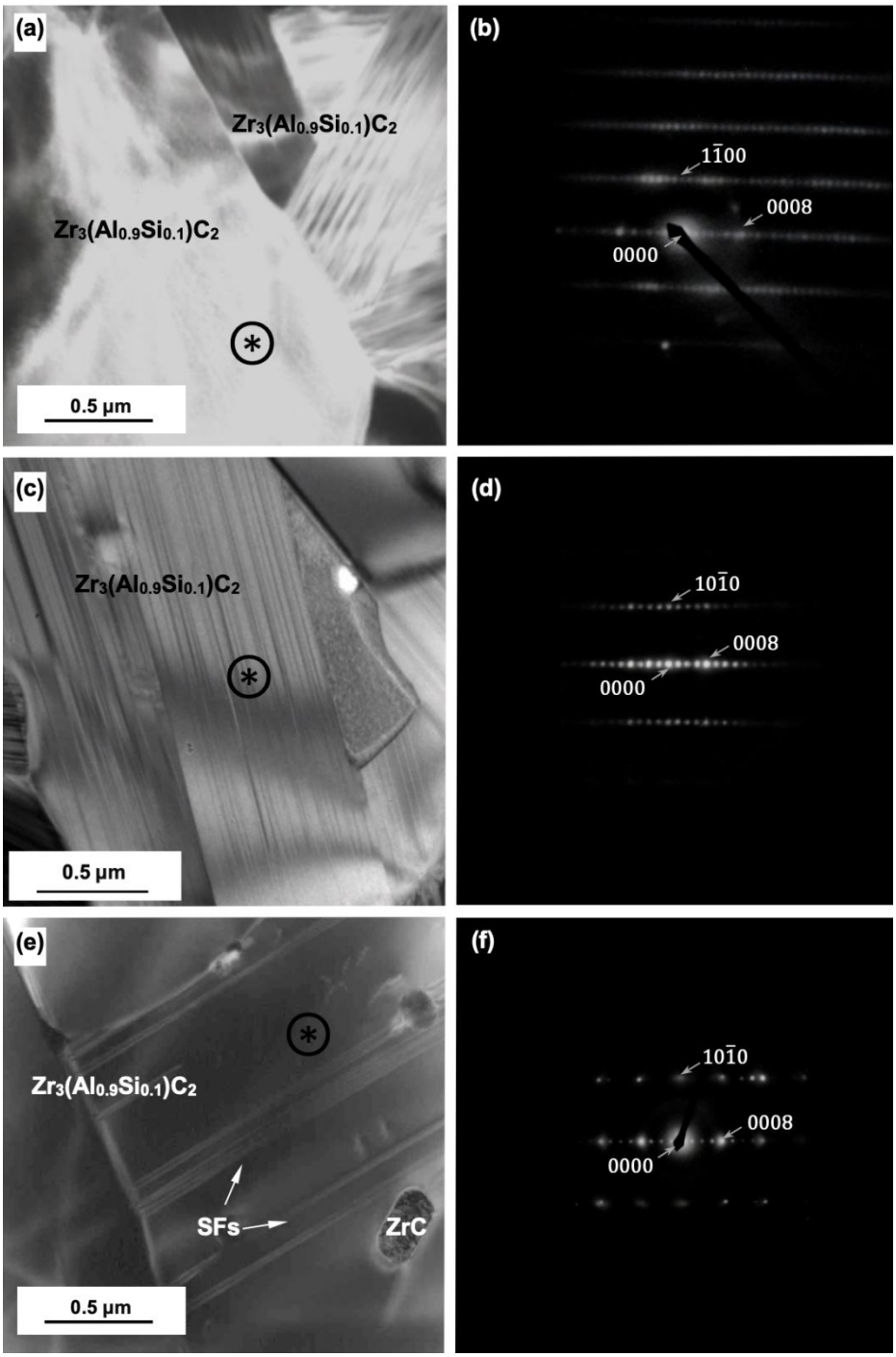

Fig. 9. Bright field images ((a), (c) and (e)) and corresponding SAED patterns ((b), (d) and (f), respectively) from the starred circular regions, obtained from $Zr_3(Al_{0.9}Si_{0.1})C_2$ grains from pristine material which had neither been irradiated nor heat treated. Stacking faults on (0001) basal planes are evident in the $Zr_3(Al_{0.9}Si_{0.1})C_2$ grains in (a), (c) and (e).

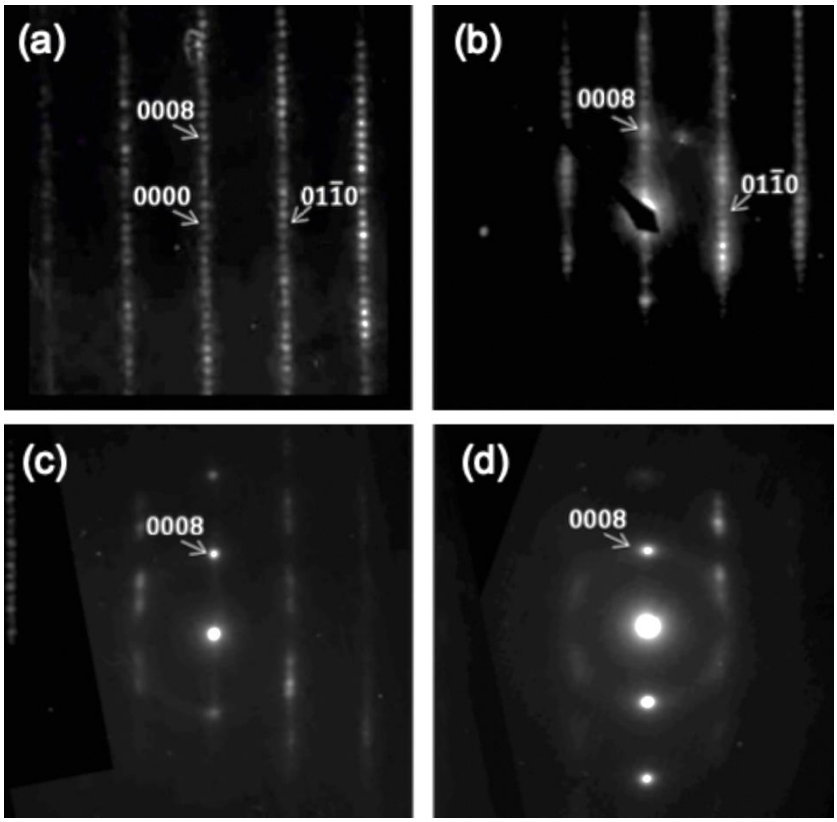

Fig. 10. SAED patterns obtained from $Zr_3(Al_{0.9}Si_{0.1})C_2$ grains irradiated with 52 MeV I^{7+} ions at RT (a) 1.5 dpa, (b) 3.5 dpa, (c) 5.0 dpa, (d) 8.0 dpa. The patterns were obtained from different samples and were taken at different zone axes, but all include the [000*l*] systematic row of reflections.

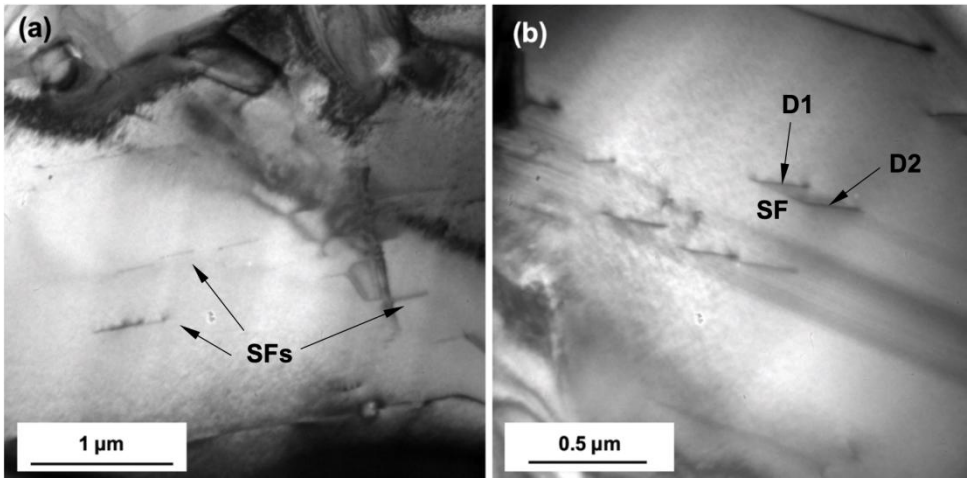

Fig. 11. Defects in $Zr_3(Al_{0.9}Si_{0.1})C_2$ irradiated to 5.0 dpa at RT: (a) parallel arrays of stacking faults along a single grain on the (000l) planes (b) Stacking fault (SF) bound by dislocations D1 and D2; these are situated within the grain and are on the (000l) planes.

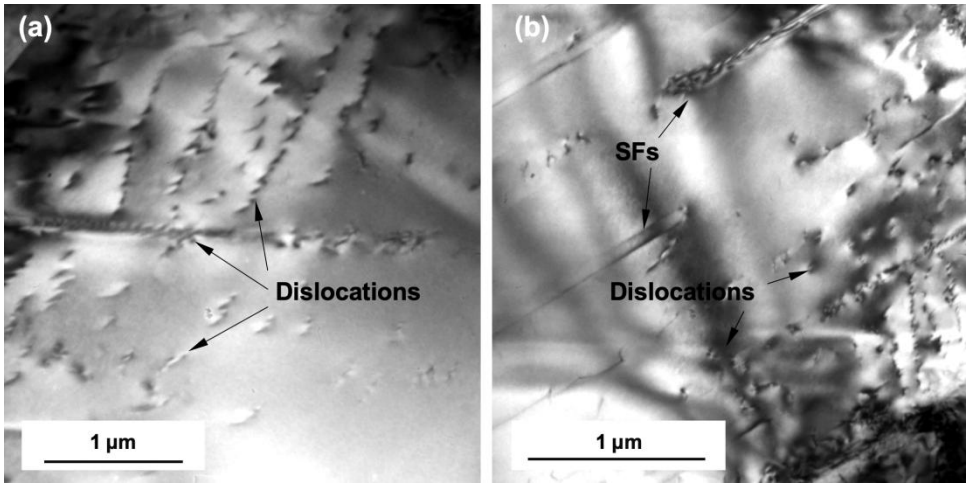

Fig. 12. Defects in $Zr_3(Al_{0.9}Si_{0.1})C_2$ irradiated to 8.0 dpa at RT and subsequently heat treated at 300°C: (a) dislocations (b) arrays of stacking faults and dislocations.

4. Discussion

The ion bombardment of atoms in a crystal lattice generally causes changes to the atomic arrangement. If the bombarding particle has sufficient energy, equal to or higher than the threshold displacement energy of the atom, the ions can displace atoms from their atomic sites. In addition, if the displaced atoms have sufficient energy, they may themselves bombard other atoms, and thus cause further atomic displacements. Defects generated by the ion cascades form vacancies and interstitials, and an accumulation of these defects can produce extended defects, such as dislocations and stacking faults, or regions of high disorder, such as regions of amorphous or poorly ordered material [19,34].

Irradiating $Zr_3(Al_{0.9}Si_{0.1})C_2$ with high energy heavy iodine ions to $\geq$ 1.5 dpa at RT resulted in several modifications to the material. The temperature at which irradiation occurs generally has a significant effect on the mobility and annihilation of defects within the crystal structure. At the temperature used for the irradiation experiments reported here on this 312 Zr MAX phase material, RT, ceramics do not tend to have a high tendency for dynamic defect annihilation, as there is a lack of thermal energy for defect migration in comparison with irradiation at higher temperatures, e.g. $\geq$300°C. This lack of mobility reduces the likelihood of defects recombining, or moving easily to low energy regions, such as the (000l) basal planes in the hexagonal structure of $Zr_3(Al_{0.9}Si_{0.1})C_2$. Under RT irradiation conditions, to 1.5 dpa, $Zr_3(Al_{0.9}Si_{0.1})C_2$ is shown to remain crystalline, but a number of defects develop in the form of stacking faults and dislocation lines. At increasingly higher irradiation doses, defects form in the crystal structure of $Zr_3(Al_{0.9}Si_{0.1})C_2$ and accumulate along select planes. A build-up of these defects can lead to the formation of further extended

defect and defect clusters, such as dislocations and stacking faults. Prolonged irradiation on the crystal generally leads to local loss of long-range order, i.e. amorphisation. At increasingly higher irradiation doses, $Zr_3(Al_{0.9}Si_{0.1})C_2$ developed more of these defects and became more disordered, as can be seen in changes to both X-ray diffraction profiles and to electron diffraction patterns containing 000*l* systematic rows of reflections. This is expected qualitatively, as more ion irradiation causes more disruption to the ordered atoms in the crystal, and more Frenkel pairs are expected to be generated by the ion cascades, causing extensive defect accumulation.

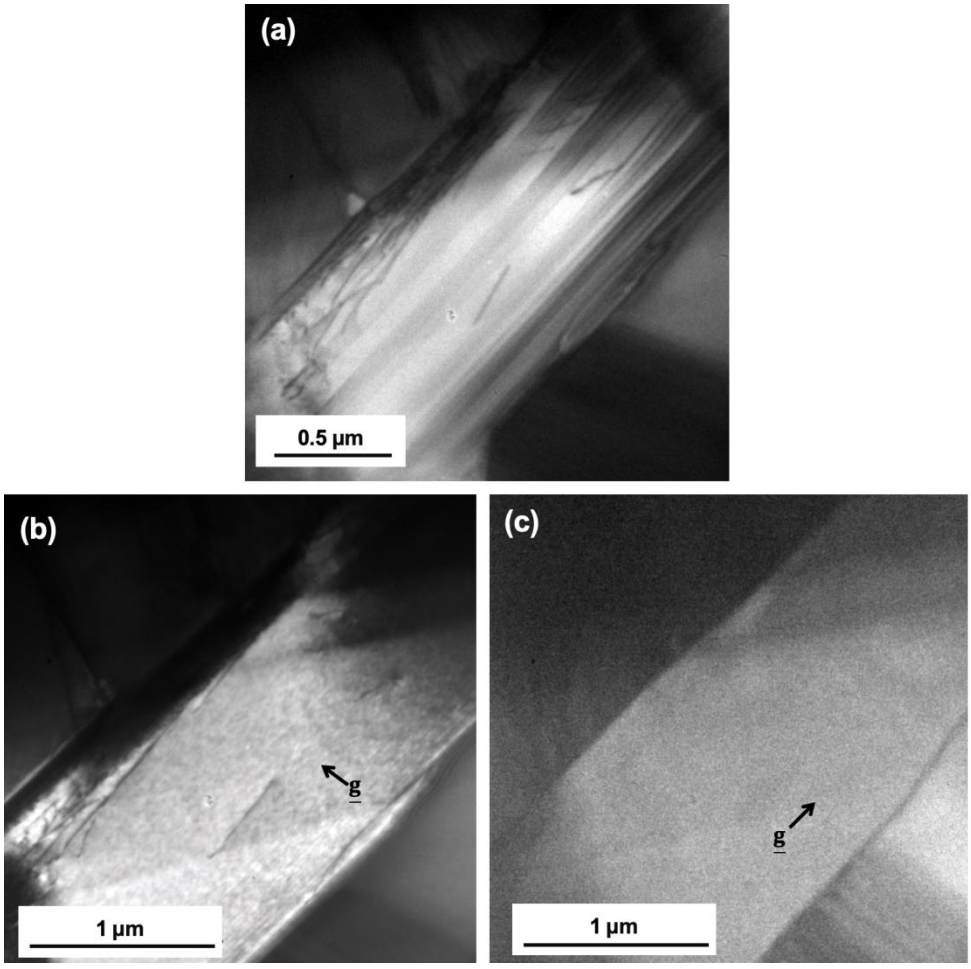

Fig. 13. Features along the (000l) axis in $Zr_3(Al_{0.9}Si_{0.1})C_2$ irradiated to 5 dpa at RT: (a) stacking faults and dislocations along the 000l planes at a general zone axis, (b) the same features of (a) but at an orientation near the $[2\bar{1}\bar{1}0]$ zone, with the stacking faults and dislocations showing less contrast, and with **g** = 0008 (c) the same features as (a) but in an orientation near the $[2\bar{1}\bar{1}0]$ zone, showing zero contrast, where the **g** vector used to form the image was $01\bar{1}0$.

Calculating the formation energies of defects is beneficial in helping to understand the consequences of defects produced by ion bombardment. Density Functional Theory (DFT) calculations on both Zr_3AlC_2 and Zr_3SiC_2 by Zapata-Solvas et al. [3] and Bowden et al. [29] show that the lowest energy intrinsic disorder mechanism in Zr_3AlC_2, with formation energies predicted to be 1.46 eV [3] or 1.51 eV [29] is the Frenkel defect in which Al ions move to interstitial sites, forming Al interstitials (Al_i) and Al vacancies (V_{Al}). This formation energy is higher than in (the hypothetical) Zr_3SiC_2, suggesting that Zr_3AlC_2 is inherently the more radiation-tolerant of the two materials [3]. However, Zapata-Solvas et al. also note the expected superior performance of the Ti-MAX phases Ti_3AlC_2 and Ti_3SiC_2 in radiation environments by comparison because in these materials the 'A' site Frenkel defect mechanism is a much higher energy mechanism, with predicted formation energies of 3.40 eV and 3.19 eV, respectively [3].

Both sets of DFT calculations also show that there is a favourable and direct route to transform Zr interstitials (Zr_i) to Zr ions on Al sites, Zr_{Al}, and Al interstitials, Al_i, in Zr_3AlC_2, and to transform Zr_i to Zr_{Si} and Si_i in Zr_3SiC_2. Therefore, after a displacement cascade induced by ion irradiation, it is reasonable to expect both Zr_{Al} and Zr_{Si} antisite defects in $Zr_3(Al_{0.9}Si_{0.1})C_2$. However, in comparison with Ti_3AlC_2, in which calculations by Zapata-Solvas et al [3] and experimental observations [35] show that antisite defects can readily exist, the concentration of antisite defects in Zr_3AlC_2 is predicted to be lower because this route is significantly less favourable energetically in Zr_3AlC_2 [3]. As Yang et al. [36] and Wang et al. [35] have noted, the formation of Ti_{Al} and Al_{Ti} antisite defects as a consequence of ion irradiation are precursor events in the phase transformation behaviour of α-Ti_3AlC_2 to β-Ti_3AlC_2. It is evident that the formation of antisite defects is a likely precursor event for the phase transformation of α-$Zr_3(Al_{0.9}Si_{0.1})C_2$ to β-$Zr_3(Al_{0.9}Si_{0.1})C_2$ found in our X-ray work.

It is important to recognise that MAX phases do not always undergo either a phase transformation or phase decomposition with relatively high dpa ion irradiation doses, even when irradiated at room temperature [10,11]. When decomposition is reported to occur, it is common for one decomposition product to be the M-metal carbide, such as TiC reported as a phase decomposition product from neutron irradiation of Ti_3AlC_2 and Ti_3SiC_2 [23] and TiC produced as a consequence of the bombardment of Ti_3SiC_2 by iodine ions nominally under ambient temperature conditions [23,37]. In general, M–X bonds are much stronger in shear in MAX phases than the M–A bonds [6], and therefore it can be rationalised that M–X bonds are more likely to withstand high energy ion bombardments than M–A bonds. This ease of breaking of M–A bonds is consistent with the relative ease of forming Al_i and V_{Al} and Si_i and V_{Si} in MAX phases.

In the work reported here, the most immediate observation from the XRD profiles in this study is the presence of strong and relatively intense ZrC peaks at all irradiation doses. While ZrC was a significant secondary phase in the material prior to irradiation, the strong reflections from ZrC seen in the XRD patterns suggest that ZrC not only remains in the material after irradiation, but that additional ZrC is formed as a product of the irradiation-induced phase transformation of $Zr_3(Al_{0.9}Si_{0.1})C_2$. The decomposition of the $Zr_3(Al_{0.9}Si_{0.1})C_2$ is shown to increase further at higher doses, which suggests this phase is sensitive to crystal damage. The lack of a change in topography of the samples at a micrometre level when observed by SEM and the progressive appearance of amorphous rings in the TEM electron diffraction patterns from MAX phase material as the level of irradiation increases together point to a gradual decomposition within the MAX phase grains at a nanometre level, leading to both the phase transformation of α-$Zr_3(Al_{0.9}Si_{0.1})C_2$ to β-$Zr_3(Al_{0.9}Si_{0.1})C_2$ and the decomposition of α-$Zr_3(Al_{0.9}Si_{0.1})C_2$ to ZrC and $Zr(Si/Al)_2$. In this context, it is also interesting to note that Bowden et al. also report the phase decomposition of non-irradiated Zr_3AlC_2 to ZrC and Zr_3Al_2 after heating above 300 °C in a nitrogen atmosphere [29].

XRD analysis from $Zr_3(Al_{0.9}Si_{0.1})C_2$ irradiated to 1.5 dpa showed that there was an expansion along the *c*-parameter, with contraction of the *a*-parameter. Although accurate lattice parameter measurements were only taken from the sample irradiated at 1.5 dpa and so a trend cannot be deduced from this single measurement, this increase in the *c*-parameter and decrease in the *a*-parameter is consistent with other irradiated MAX phase work on Ti-based MAX phases [26,27] and also the recent proton irradiation work on Zr_3AlC_2 of Bowden et al. [29]. It would clearly be interesting to see whether heavy ion irradiation of this MAX phase at higher temperatures would help to reduce the number of cracks seen, as Bowden et al. reported in their work [29], and thereby determine the relationship of lattice swelling to macroscopic volume swelling of material. However, such work would require significantly higher purity MAX phase material for irradiation work.

In contrast to Ti_3SiC_2 where heat treatment at 560 °C for 1 hr of Ti_3SiC_2 bulk material irradiated with 2 MeV I^{2+} enables crystal regrowth of both Ti_3SiC_2 and TiC, one of the decomposition products produced after irradiation, [37], heat treatment of our MAX-phase-rich material for 1 hr at both 300 °C and 600 °C did not produce any noticeable change to the material. It is entirely possible that this can only occur for heat treatments at higher temperatures, but unfortunately, the limited amount of material that we had available for study precluded further, higher temperature heat treatments of longer time.

Ideally, Zr_3AlC_2 samples would have been the most suitable samples to study. Previous work on the synthesis of this phase and $Zr(Al_{1-x}Si_x)C_2$ has shown how difficult it is to produce material with significant weight fractions of MAX phase

[1,3,29]. Thus, for example, the material produced by Lapauw et al. [1] contained 61 mol% Zr_3AlC_2, 31 mol% ZrC and 8 mol% $ZrAl_2$, and the $Zr(Al_{0.9}Si_{0.1})C_2$ material produced by Zapata-Solvas et al. [3] actually contained 59 ± 2 wt% of $Zr(Al_{0.9}Si_{0.1})C_2$, with significant quantities of ZrC (31 ± 2 wt%), $ZrAl_2$ (5 ± 1 wt%) and Zr_5Si_3 (5 ± 1 wt%). Zapata-Solvas reported that the introduction of trace levels of Si helps in the formation of this MAX phase. Bowden et al. noted how Ti stabilises the Zr_3AlC_2 MAX phase [29]. The fact that it has proved difficult to produce significantly higher purity levels of $Zr_3(Al_{1-x}Si_x)C_2$ material suggests that this phase may not be a thermodynamically stable phase in the Zr–(Al,Si) –C phase diagram, in contrast to the Ti–Al –C phase diagram where Ti_3AlC_2 is definitely regarded as a stable phase, albeit a high temperature phase stable within a relatively narrow temperature range [38,39]. Clearly, it would be beneficial to have to hand a reliable phase diagram for the Zr–(Al,Si) –C quaternary system and an understanding of how to reliably produce significant quantities of high wt% Zr_3AlC_2-based MAX phase for future irradiation studies.

Despite the constraints imposed on this study by having a relatively small quantity of material with only 68 wt% $Zr_3(Al_{0.9}Si_{0.1})C_2$ to undertake all our experiments, the SEM, TEM and XRD data together clearly suggest that the response of this MAX phase to high dose heavy ion irradiation at room temperature is complex. Further work is required to establish under what conditions it might be possible to consider this material for use in future nuclear reactor environments.

5. Conclusions

Zirconium-based MAX phase with the composition $Zr_3(Al_{0.9}Si_{0.1})C_2$, in material also containing ZrC and Zr_5Si_3, has been irradiated at RT with 52 MeV I^{9+} ions, reaching an estimated damage level of up to 8.0 dpa. Post-irradiation characterisation of the damaged region was carried out using TEM, SEM and XRD. Examination of irradiated $Zr_3(Al_{0.9}Si_{0.1})C_2$ suggests that it demonstrates a poor resistance to ion irradiation at these relatively high doses and relatively low temperature conditions. At the highest doses, the MAX phase decomposed into nanoregions of ZrC, $Zr(Al,Si)_2$ and also transformed into a polymorph with a new stacking structure, identified by XRD as β-$Zr_3(Al,Si)C_2$.

Acknowledgements

This work was financially supported by the Engineering and Physical Sciences Research Council (EPSRC) United Kingdom, under contract EP/M018768/1. We are grateful to the referees of our original manuscripts for their very useful constructive comments on our work.

Data Availability

The raw/processed data required to reproduce these findings cannot be shared at this time as the data also forms part of an ongoing study.

References

[1] T. Lapauw, J. Halim, J. Lu, T. Cabioc'h, L. Hultman, M.W. Barsoum, K. Lambrinou, J. Vleugels, Synthesis of the novel Zr_3AlC_2 MAX phase, J. Eur. Ceram. Soc. 36 (2016) 943–947.

[2] T. Lapauw, K. Lambrinou, T. Cabioc'h, J. Halim, J. Lu, A. Pesach, O. Rivin, O. Ozeri, E.N. Caspi, L. Hultman, P. Eklund, J. Rosén, M.W. Barsoum, J. Vleugels, Synthesis of the new MAX phase Zr_2AlC, J. Eur. Ceram. Soc. 36 (2016) 1847–1853.

[3] E. Zapata-Solvas, S-R.G. Christopoulos, N. Ni, D.C. Parfitt, D. Horlait, M.E. Fitzpatrick, A. Chroneos, W.E. Lee, Experimental synthesis and density functional theory investigation of radiation tolerance of $Zr_3(Al_{1-x}Si_x)C_2$ MAX phases, J. Am. Ceram. Soc. 100 (2017) 1377–1387.

[4] A. Joulain, L. Thilly, J. Rabier, Revisiting the defect structure of MAX phases: the case of Ti_4AlN_3, Philos. Mag. 88 (2008) 1307–1320.

[5] M.W. Barsoum, MAX Phases: Properties of Machinable Ternary Carbides and Nitrides, Wiley-VCH GmbM & co. KGaA, Weinheim, Germany 2013.

[6] M.W. Barsoum, M. Radovic, Elastic and mechanical properties of the MAX phases, Annu. Rev. Mater. Res. 41 (2011) 195–227.

[7] T. El-Raghy, S. Chakraborty, M.W. Barsoum, Synthesis and characterization of Hf_2PbC, Zr_2PbC and M_2SnC (M = Ti, Hf, Nb or Zr), J. Eur. Ceram. Soc. 20 (2000) 2619–2625.

[8] I.M. Low, Y. Sakka, C.F. Hu, MAX phases and ultra-high temperature ceramics for extreme environments, IGI Global, Hershey, Pennsylvania 2013.

[9] H. Gutzmann, F. Gärtner, D. Höche, C. Blawert, T. Klassen, Cold spraying of Ti_2AlC MAX-phase coatings, J. Therm. Spray Technol. 22 (2013) 406–412.

[10] J.C. Nappé, P. Grosseau, F. Audubert, B. Guilhot, M. Beauvy, M. Benabdesselam, I. Monnet, Damages induced by heavy ions in titanium silicon carbide: Effects of nuclear and electronic interactions at room temperature, J. Nucl. Mater. 385 (2009) 304–307.

[11] K.R. Whittle, M.G. Blackford, R.D. Aughterson, S. Moricca, G.R. Lumpkin, D.P. Riley, N.J. Zaluzec, Radiation tolerance of $M_{n+1}AX_n$ phases, Ti_3AlC_2 and Ti_3SiC_2, Acta Mater. 58 (2010) 4362–4368.

[12] J.C. Nappé, I. Monnet, F. Audubert, P. Grosseau, M. Beauvy, M. Benabdesselam, Formation of nanosized hills on Ti_3SiC_2 oxide layer irradiated with swift heavy ions, Nucl. Instr. Meth. Res. B 270 (2012) 36–43.

[13] P. Song, J.R. Sun, Z.G. Wang, M.H. Cui, T.L. Shen, Y.F. Li, L.L. Pang, Y.B. Zhu, Q. Huang, J.J. Lü, Irradiation resistance properties studies on helium ions irradiated max phase Ti_3AlC_2, Nucl. Instr. Meth. Res. B 326 (2014) 332–336.

[14] K.L. Murty, I. Charit, An Introduction to Nuclear Materials, Wiley-VCH GmbM & co. KGaA, Weinheim, Germany 2015.

[15] C.R.F. Azevedo, Selection of fuel cladding material for nuclear fission reactors, Eng. Fail. Anal. 18 (2011) 1943–1962.

[16] G.S. Was, Fundamentals of Radiation Materials Science, 2nd Edition, Springer-Verlag GmbH Berlin Heidelberg, 2017.

[17] X.M. Liu, M. Le Flem, J.-L. Béchade, F. Onimus, T. Cozzika, I. Monnet, XRD investigation of ion irradiated $Ti_3Si_{0.90}Al_{0.1}0C_2$, Nucl. Instr. Meth. Res. B 268 (2010) 506–512.

[18] M. Le Flem, X.M. Liu, S. Doriot, T. Cozzika, I. Monnet, Irradiation damage in $Ti_3(Si,Al)C_2$: a TEM investigation, Int. J. Appl. Ceram. Technol. 7 (2010) 766–775.
[19] L.W. Hobbs, F.W. Clinard, S.J. Zinkle, R.C. Ewing, Radiation effects in ceramics, J. Nucl. Mater. 216 (1994) 291–321.
[20] H.G van Bueren, Elektrischer Widerstand und plastische Deformation von Metallen, Z. Metall. 46 (1955) 272–282.
[21] A.K. Seeger, Some recollections of the radiation damage work of the 1950s, Proc. Roy. Soc. Lond. A 371 (1980) 165–172.
[22] K. Trachenko, Understanding resistance to amorphization by radiation damage, J. Phys.: Cond. Matt. 16 (2004) R1491–R1515.
[23] D.J. Tallman, E.N. Hoffman, E.N. Caspi, B.L. Garcia-Diaz, G. Kohse, R.L. Sindelar, M.W. Barsoum, Effect of neutron irradiation on select MAX phases, Acta Mater. 85 (2015) 132–143.
[24] C. Ang, S. Zinkle, C.H. Shih, C. Silva, N. Cetiner, Y. Katoh, Phase stability, swelling, microstructure and strength of Ti_3SiC_2-TiC ceramics after low dose neutron irradiation, J. Nucl. Mater., 483 (2017) 44–53.
[25] C. Ang, C.M. Parish, C.H. Shih, C. Silva, Y. Katoh, Microstructure and mechanical properties of titanium aluminum carbides neutron irradiated at 400−700°C, J. Eur. Ceram. Soc. 37 (2017) 2353−2363.
[26] Q. Huang, R.D. Liu, G.H. Lei, H.F. Huang, J.J. Li, S.X. He, D.H. Li, L. Yan, J. Zhou, Q. Huang, Irradiation resistance of MAX phases Ti_3SiC_2 and Ti_3AlC_2: Characterization and comparison, J. Nucl. Mater. 465 (2105) 640–647.
[27] D.W. Clark, S.J. Zinkle, M.K. Patel, C.M. Parish, High temperature ion irradiation effects in MAX phase ceramics, Acta Mater. 105 (2016) 130–146.
[28] H.H. Qarra, K.M. Knowles, M.E. Vickers, S. Akhmadaliev, K. Lambrinou, Heavy ion irradiation damage in Zr_2AlC MAX phase, J. Nucl. Mater. 523 (2019) 1–9.
[29] D. Bowden, J. Ward, S. Middleburgh, S. de Moraes Shubeita, E. Zapata-Solvas, T. Lapauw, J. Vleugels, K. Lambrinou, W.E. Lee, M. Preuss, P. Frankel, The stability of irradiation-induced defects in Zr_3AlC_2, Nb_4AlC_3 and $(Zr_{0.}5,Ti0_{.5})_3AlC_2$ MAX phase-based ceramics, Acta Mater. 183 (2020) 24−35.
[30] S. Akhmadaliev, R. Heller, D. Hanf, G. Rugel, S. Merchel, The new 6 MV AMS-facility DREAMS at Dresden, Nucl. Instr. Meth. Res. B 294 (2013) 5–10.
[31] L.A. Giannuzzi, F.A. Stevie, A review of focused ion beam milling techniques for TEM specimen preparation, Micron. 30 (1999) 197–204.
[32] L. Farber, I. Levin, M.W. Barsoum, T. El-Raghy, T. Tzenov, High-resolution transmission electron microscopy of some $Ti_{n+1}AX_n$ compounds (n=1, 2; A=Al or Si; X=C or N), J. Appl. Phys. 86 (1999) 2540–2543.
[33] K.M. Knowles and M.V. Ravichandran, Structural analysis of inclusions in β-silicon carbide whiskers grown from rice hulls, J. Am. Ceram. Soc. 80 (1997) 1165–1173.
[34] K. Nordlund, S.J. Zinkle, A.E. Sand, F. Granberg, R.S. Averback, R.E. Stoller, T. Suzudo, L. Malerba, F. Banhart, W.J. Weber, F. Williame, S.L. Dudarev and D. Simeone, Primary radiation damage: A review of current understanding and models, J. Nucl. Mater. 512 (2018) 450–479.
[35] C.X. Wang, T.F. Yang, C.L. Tracy, C.Y. Lu, H. Zhang, Y-J. Hu, L.M. Wang, L. Qi, L. Gu, Q. Huang, J. Zhang, J.Y. Wang, J.M. Xue, R.C. Ewing and Y.G.

Wang, Disorder in $M_{n+1}AX_n$ phases at the atomic scale, Nature Communications 10 (2019) 622 (9 pp.).

[36] T.F. Yang, C.X. Wang, C.A. Taylor, X.J. Huang, Q. Huang, F.Z. Li, L. Shen, X.B.. Zhou, J.M. Xue, S. Yan and Y.G. Wang, The structural transitions of Ti_3AlC_2 induced by ion irradiation, Acta Mater. 65 (2014) 351–359.

[37] L. Zhang, Q. Qi, L.Q. Shi, D.J. O'Connor, B.V. King, E.H. Kisi, D.K. Venkatachalam, Damage tolerance of Ti_3SiC_2 to high energy iodine irradiation, Appl. Surf. Sci. 258 (2012) 6281–6287.

[38] D. Bandyopadhyay, R.C. Sharma and N. Chakraborti, The Ti-Al-C system (titanium - aluminum - carbon), J. Phase Equil. 21 (2000) 195–198.

[39] V. Raghavan, Al-C-Ti (aluminum-carbon-titanium) J. Phase Equi. Diff. 27 (2006) 148–149.